Towards thermo- and superlubricity on the macroscopic scale: from nanostructures to graphene and graphite lubrication

Antonov, P.V.; Antonov P.V.

Chapter 3

Fabrication of high-aspect ratio silicon nanopillars for tribological experiments

3.1 Introduction

3.1.1 Overview of relevant nanomanufacturing techniques

Over the past decade, nanostructured surfaces have become widely used in electronics [1], biomedicine [2], photonic crystals [3], battery technology [4], solar cells [5], etc. Independently of the area of application, the most important points of interest of nanofabrication control are the shapes that can be manufactured, including the aspect ratios of extreme shapes such as nanopillars (NPs), and the reproducibility with which the final structures can be produced.

From a technological point of view, the manufacturing process of NPs over macroscopic areas presents a relatively complex task, even though a wide range of literature is available describing various methods for producing NP arrays. As an example, the traditional method of so-called 'natural lithography' [7,8] serves as a flexible and affordable technological platform, both technically and economically, that provides good control over the pitch and sharpness of the structures [9,12]. The natural lithography method employs self-assembly of nano- or microparticles from a solution that is spin-coated on top of the substrate. The resulting layer of particles serves as a mask for the subsequent process of etching. However, it is not possible to avoid irregularities due to the uneven distribution in the self-assembled pattern of particles. The latter may result in height variations after etching, thus inhomogeneity in the nanopillar array.

Conventional ultraviolet- (UV) and holography-based lithography could also be effective approaches [23]. Generally, these methods are based on the optical projection of a geometrical pattern from a photomask, directly to the substrate that is coated with a photoresist. With this method, modifications in the final structures (size, shape, distribution) are restricted, because one needs to fabricate a separate photomask for each pattern, which is costly. Moreover, conventional cleanroom ultraviolet lithography (instead of deep or extreme ultraviolet) delivers a resolution of $\sim 0.5\,\mu m$ [10, 11]. This modest resolution may not be sufficient to produce nanopillars, which, in our case, have to be as small as $50\,nm$ in diameter.

Another conventional method is nanoimprint lithography [13, 22]. Conceptually the method employs the imprinting of a nanoscale template ('stamp') onto the substrate ('replica') under the action of a certain normal force. Recently, an

extreme vertical resolution below 2 nm was achieved with this method [22]. On the other hand, similar to the case of UV lithography, this method requires separate stamps for different patterns.

These factors explain our preference for electron beam lithography [14-16]. With this method, it is possible to produce large areas, up to several square centimeters, of round shape patterns with a precision of $2 \div 5\ nm$. Electron beam lithography enables us to manufacture these NP patterns following well-established recipes and to reach high quality and reproducibility. The versatility of this method is also due to the fact that an electron beam can directly write any desired pattern in an electron-beam-sensitive resist layer. Therefore, no photomasks or stamps are needed.

3.2 NP fabrication

Figure 3.1 shows schematically the main steps of the NP fabrication process. As substrates, we used $10 \times 10\ mm^2$ pieces of Si(100) wafer (p-type). Prior to processing, samples were cleaned in two steps. Firstly, they were placed for 5 min in acetone in an ultrasonic bath and were then rinsed with DI water. Secondly, the samples were transferred to a fuming nitric acid (99.9%) HNO_3 bath and kept there for 7 min. They were then rinsed with DI water and dried with N_2. In order to remove residual moisture, the Si samples were baked for 2 min at $250°C$. To write a pattern on the Si samples we used a negative tone hydrogen silsesquioxane (HSQ) resist (XR-1541 Dow Corning, 6% in H_2O). This particular choice is motivated by two factors: first, this resist provides a high resolution and a high selectivity during its exposure to the electron beam in the Electron beam pattern generator (EBPG); second, it has a subsequent low etch rate [7], which enables etching of the high-aspect-ratio NPs. The HSQ resist was first heated to room temperature, after which it was applied directly to the Si substrate, as it did not require any primer due to its strong atomic binding to the substrate. Spin coating was conducted for 55 sec at rotation speeds in the range of 4000 to 5500 RPM, depending on the required aspect ratio of the pillars. The final resist layer thickness ranged between 80 nm at low rotation speeds and 60 nm at high speeds.

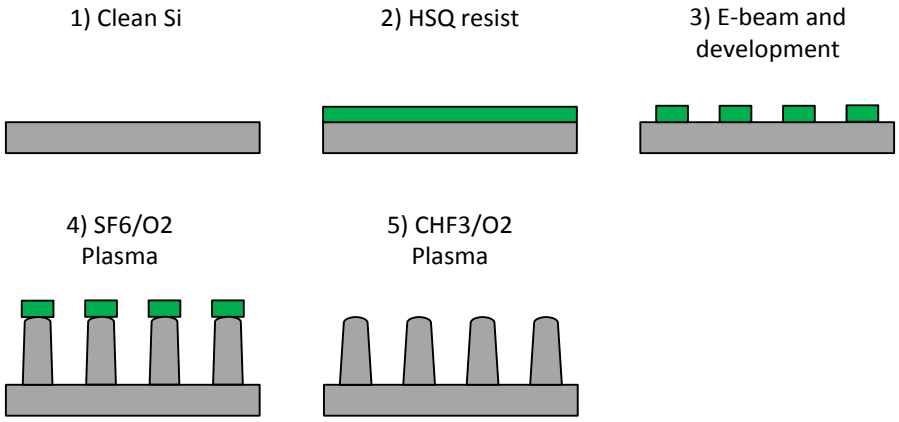

Figure 3.1. Schematic of the step-by-step fabrication process of the NP arrays.

To obtain a high lithography contrast, the samples were then baked at 80°C for 4 min. The nanopatterns were written in the HSQ layer by means of a Vistec 5000+ Electron Beam Pattern Generator (EBPG). The thinnest NPs that we have manufactured, had a diameter of 50 nm. All patterns were specified by use of the AutoCAD 2013 program and then converted to the corresponding EBPG format. Typically, each of the NP arrays was generated over an area of 50× 50 μm^2. Optimum resolution was achieved for an electron dose of approximately 1950 $\mu C/cm^2$ at an acceleration voltage of 100 kV. After exposure, the patterns were developed in a 25% tetramethylammonium hydroxide solution (TMAH) in H_2O for 30 sec at a temperature of 80°C. Immediately afterwards the samples were carefully rinsed with DI water for 30 sec and flushed with N_2. We have used cryogenic Deep Reactive Ion Etching (DRIE) to etch the pillars. This technique is the most powerful and precise method for manufacturing high-aspect-ratio structures in Si [11, 17-19]. The etching was carried out in an Adixen AMS-100 Plasma Etcher. The discharge was generated by an RF Inductively Coupled Plasma (ICP) source, directly connected to the working chamber, as shown in Fig. 3.2. The second RF source was connected directly to the specimen table, to provide sufficient directional ion bombardment onto the surface of the sample.

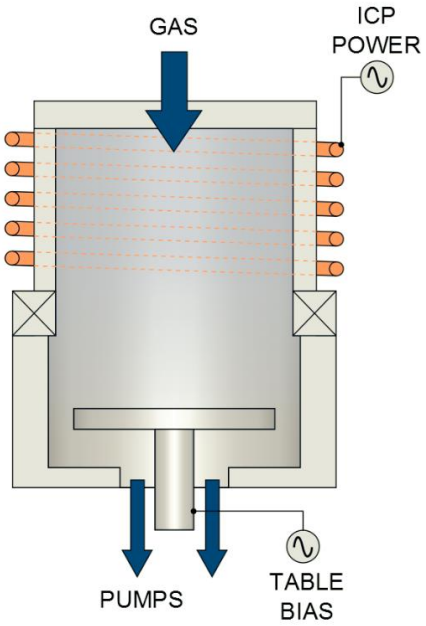

Figure 3.2. Schematic of RF Inductively Coupled Plasma system [21], used for the Deep Reactive Ion Etching of the NP patterns.

The sample was clamped to a cryogenic holder that was cooled by a flow of liquid N_2. Helium was back-streamed below the holder in order to provide enough thermal contact between the sample and the holder so as to maintain a working temperature of $-120°C \pm 0.5°C$. SF_6 was chosen as the working gas, as this provides active fluorine atoms on the sample to react and form an etching product with Si, which is volatile SiF_4. Oxygen was added to the SF_6, in order to passivate the sidewalls of the vertical structures during etching and thus avoid potential undercut. The optimal gas flow ratio for this process was established experimentally as $SF_6 : O_2 = 6.7 : 1$; specifically, the flow rate of SF_6 was 200 $sccm$ and that of O_2 was 30 $sccm$, at a total chamber pressure of 6 $mbar$. An important point to note is that the optimal oxygen gas flow depended strongly on the size of the individual NP, their density on the surface and the exposed area of the silicon sample. The RF power was set to 1100 W, and the bias voltage to $-40V$. With these moderate conditions we achieved a typical etch rate of Si of approximately

2400 nm/min with a selectivity of 80:1 with respect to the HSQ resist. This process produced NP arrays with varying aspect ratios (Fig. 3.3).

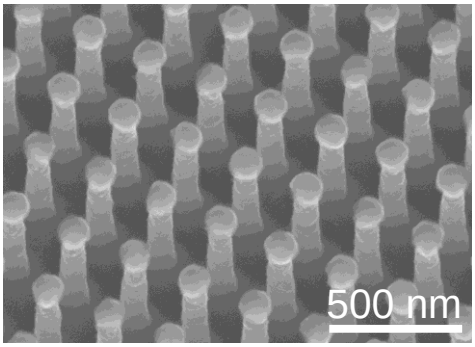

(a)

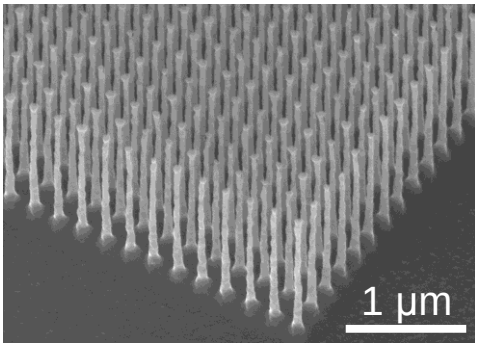

(b)

Figure 3.3. Scanning electron microscopy images of arrays of Si NPs with different aspect ratios. a) Aspect ratio 1:4, pillar diameter 95 nm*, pillar length* 400 nm*, pitch between pillar centers* 250 nm*. b) Aspect ratio 1:24, pillar diameter* 55 nm*, pillar length* 1.35 μm*, pitch* 200 nm*. Note the resist residue, decorating the top of each NP.*

3.3 Removal of resist residues

Since the prime objective of producing these structures was to study their tribological (i.e. frictional) properties, it was important to have control over the shape, composition and mechanical properties of the apices of the pillars. This issue was addressed in combination with the removal of the resist residues that remained on top of the pillars after the DRIE procedure. We considered three options for the removal of the HSQ residues. The first option was to dissolve these residues, which are chemically similar to SiO_2, in a hydrofluoric acid solution. We found that a 7% buffered HF solution readily dissolved the HSQ residues, as was expected, but that this treatment had a deleterious effect on the shapes of the pillars, especially for aspect ratios more extreme than 1:12. After HF etching, these had become very rough. In turn, certain pillars, which had undergone the under-etching effect below the resist after the DRIE (see Fig. 3.3a), showed an inhomogeneous height distribution after etching. Their thin top part had the smallest diameter, which thus was etched away faster than the thicker bottom part.

The second option was to use wet etching of the pillars themselves, in order to shrink their diameter uniformly, until the residues would detach. It was reported in [20] that it is possible to slowly and uniformly shrink the diameter of pillars by etching them in dilute aqua regia. In line with the recipe of Ref. [20], we immersed our samples in a solution of HNO_3 : HCl : H_2O = 1 : 3: 6 (volume fractions) for approximately 12 hours. However, the result showed a negligible etch rate and did not provide any significant changes. We speculate that the DRIE etching at $-120°C$ with O_2 for passivation had provided extra smooth side faces with low densities of chemically active sites, which could have resulted in the negligible effect of dilute aqua regia on the NPs.

The third and only successful option was to again resort to the method of plasma etching. Utilizing an inductively coupled CHF_3 plasma in combination with O_2 for passivation provided the required combination of high anisotropy and selectivity between silicon dioxide and silicon. The etching process was conducted in a Leybold Heraeus Plasma Etcher at room temperature. The following etching parameters were found to achieve the optimal result: a flow of 50 sscm CHF_3 and 2.5 $sccm$ O_2, 50 W RF power and $-680\,V$ bias voltage, at a typical, total pressure of 6 to 7 $mbar$. Under these conditions, the etch rate of silicon dioxide was approximately 36 nm/min, while that of silicon was some 3 times lower. This method allowed us to avoid excess undercut and to sharpen the pillars from the top. In Fig. 3.4 we demonstrate this effect for the example of pillars with an aspect ratio of 1:10. A minor smoothening effect was observed on the pillars during the etching process. We note that this treatment had a deleterious effect on the shapes of pillars with extreme aspect ratios, such as 1:24 (not shown here). That is why we decided not to (completely) remove the HSQ residues for those pillars. Depending on the etching time, the average radius of curvature of the apices of the pillars with aspect ratios less extreme than 1:10 varied from approximately 30 nm to 12 nm. This effect is illustrated in Fig. 3.5 for the case of NPs with an aspect ratio of 1:10.

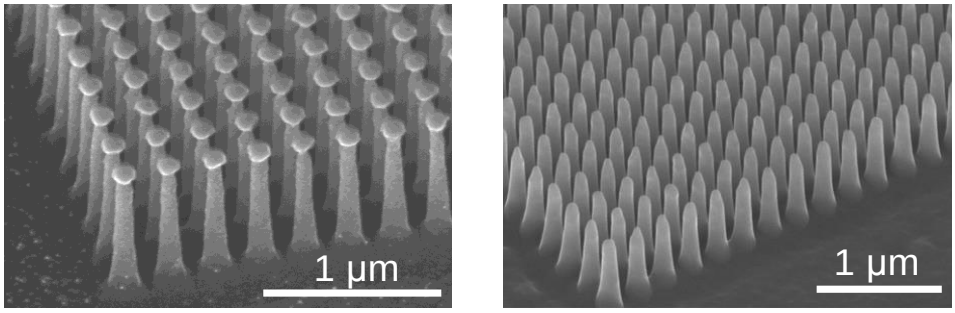

(a) (b)

Figure 3.4. Scanning electron microscopy images, illustrating the effect of CHF_3/O_2 etching. On the left are the pillars before etching, with aspect ratio 1:10, pillar length 800 nm, pillar diameter 80 nm, pitch 200 nm. Each pillar is still decorated by a residue of the resist. The image on the right shows the result after etching. Note that the resist residues have been removed and that the pillars are slightly rounded at their apex.

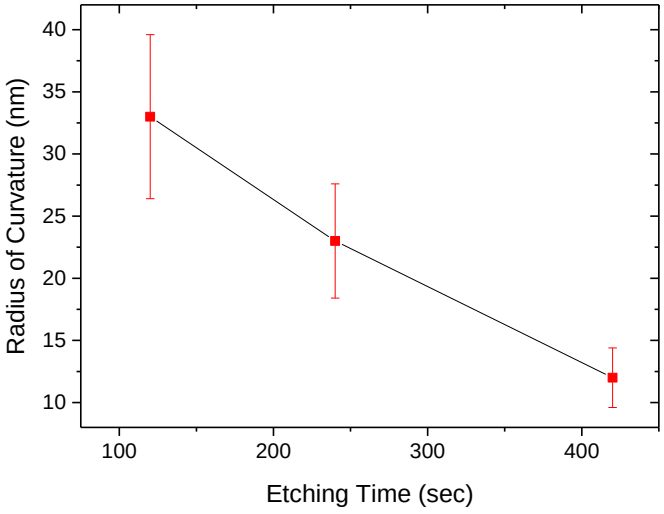

Figure 3.5. Average radius of curvature of the apices of NPs with an aspect ratio of 1:10, plotted as a function of CHF_3/O_2 etching time.

3.4 Summary

In conclusion, we have shown that DRIE at cryogenic temperatures can be used to produce large, highly reproducible and well-ordered arrays of nanopillars with various width : length aspect ratios up to 1:24 over distances of at least 50 μm. We have also applied reactive-ion plasma etching to vary the shape of the pillar apices by means of etching of the HSQ resist residues. In combination with e-beam lithography, the method shows excellent versatility, anisotropy and selectivity. In Chapter 2, the produced nanostructures are used to study their tribological properties, in an attempt to reduce dry, unlubricated friction by means of the effect of thermolubricity.

3.5 Bibliography

1. Ko H. *et al.* Multifunctional, flexible electronic systems based on engineered nanostructured materials, *Nanotechnology* **23**, 344001 (2012)
2. de Souza Antunes, A.M. *et al.* Trends in nanotechnology patents applied to the health sector, *Recent Patents on Nanotechnology* **6**, pp. 29-43 (2012).
3. Kiraly, B., Yang, S.K. & Huang, T.J., Multifunctional Porous Silicon NP Arrays, *Nanotechnology* **24**, 245704 (2013)
4. Chan, C.K. *et al*. "High-performance lithium battery anodes using silicon nanowires", *Nat. Nanotechnology* **3**, 31 (2008)
5. Liang, D. *et al*. High-Efficiency Nanostructured Window GaAs Solar Cells, *Nano Letters* **13**, pp. 4850-4856 (2013)
6. Krylov, S.Yu. & Frenken, J.W.M. The physics of atomic-scale friction: basic considerations and open questions, *Phys. Status Solidi B* **251**, 711 (2014)
7. Deckman, H.W. & Dunsmuir, J.H. Nanosphere lithography: A materials general fabrication process for periodic particle array surfaces, *Applied Physics Letters* **41**, 377 (1982)
8. Chitu, L. *et al*. Modified Langmuir-Blodgett deposition of nanoparticles - measurement of 2D to 3D ordered arrays, *Measurement Science Review* **10**, 5 (2010)
9. Hsu, C.-M., Wafer-scale silicon NPs and nanocones by Langmuir–Blodgett assembly and etching, *Applied Physics Letters* **93**, 133109 (2008)
10. Ito, T. & Okazaki, S., Pushing the limits of lithography, *Nature* **406**, 1027-31 (2000)
11. Hung, Y.-J. *et al*. Fabrication of Highly –ordered Silicon Nanowire Arrays with Controllable Sidewall Profiles for Achieving Low Surface Reflection, *Mater. Res. Soc. Symp. Proc*. **1258** (2010)
12. Huang, Z. "Fabrication of Silicon Nanowire Arrays with Controlled Diameter, Length, and Density", *Advanced Materials* **19**, pp. 744-748 (2007)
13. Torres, C.M.S. *et al*. "Nanoimprint lithography: an alternative nanofabrication approach", Mater. Sc. Eng. C **23**, pp. 23-31 (2003)
14. Vieu, C. *et al.* Electron beam lithography: resolution limits and applications, *Applied Surface Science* **164**, pp. 111-117 (2000)

15. Kaleli, B. *et al*. Electron Beam Lithography of HSQ and PMMA Resists and Importance of their Properties to Link the Nano World to the Micro World, *STW ICT Conference 2010*, Veldhoven, The Netherlands (18-19 Nov 2010)
16. Grigorescu, A.E., van der Krogt, M.C. & Hagen, C.W. Limiting factors for electron beam lithography when using ultra-thin hydrogen silsesquioxane layers, *Proceedings of SPIE* **6519** (2007)
17. Tachi, S. *et al*. Low-temperature reactive ion etching and microwave plasma etching of silicon, *Applied Physics Letters* **52**, 616 (1988)
18. Liu, Z. *et al*. Super-selective cryogenic etching for sub-10 nm features, *Nanotechnology* **24**, 015305 (2013)
19. Boufnichel, M. et al. Profile control of high aspect ratio trenches of silicon. Effect of process parameters on local bowing, *Journal Vacuum Science Technology* B **20**, pp. 1508-1513 (2002)
20. Chang, Y.-F. *et al*. Fabrication of high-aspect-ratio silicon NP arrays with the conventional reactive ion etching technique", *Appl. Phys*. A **86**, pp. 193-196 (2007)
21. Web-source: http://www.oxford-instruments.com/products/etching-deposition-and-growth/plasma-etch-deposition/icp-etch
22. Wang, X. *et al*. High resolution 3D NanoImprint technology: Template fabrication, application in Fabry–Pérot-filter-array-based optical nanospectrometers, *Microelecronic Engineering* **110**, pp. 44-51 (2013)
23. Totzeck, M. *et al*. Semiconductor fabrication: Pushing deep ultraviolet lithography to its limits, *Nature Photonics* **1**, pp. 629-631 (2007)